HHS Public Access

Author manuscript

Dev Cell. Author manuscript; available in PMC 2022 October 11.

Published in final edited form as:

Dev Cell. 2021 October 11; 56(19): 2712–2721.e4. doi:10.1016/j.devcel.2021.08.010.

Tumor-induced disruption of the blood-brain barrier promotes host death

Jung Kim[1], **Hsiu-Chun Chuang**[1], **Natalie K. Wolf**[1], **Christopher J. Nicolai**[1], **David H. Raulet**[1], **Kaoru Saijo**[1,2], **David Bilder**[1,*]

[1]Department of Molecular and Cell Biology, University of California-Berkeley, Berkeley CA, 94720, USA

[2]Helen Wills Neuroscience Institute, University of California-Berkeley, Berkeley CA, 94720, USA

SUMMARY

Cancer patients often die from symptoms that manifest at a distance from any tumor. Mechanisms underlying these systemic physiological perturbations, called paraneoplastic syndromes, may benefit from investigation in non-mammalian systems. Using a non-metastatic Drosophila adult model, we find that malignant tumor-produced cytokines drive widespread host activation of JAK-STAT signaling and cause premature lethality. STAT activity is particularly high in cells of the blood-brain barrier (BBB), where it induces aberrant BBB permeability. Remarkably, inhibiting STAT in the BBB not only rescues barrier function but also extends the lifespan of tumor-bearing hosts. We identify BBB damage in other pathological conditions that cause elevated inflammatory signaling, including obesity and infection, where BBB permeability also regulates host survival. IL-6-dependent BBB dysfunction is further seen in a mouse tumor model, and it again promotes host morbidity. Therefore, BBB alterations constitute a conserved lethal tumor-host interaction that also underlies other physiological morbidities.

Graphical Abstract

*Corresponding author and Lead contact: bilder@berkeley.edu.

AUTHOR CONTRIBUTIONS

J.K. and D.B. designed Drosophila experiments. J.K. performed Drosophila experiments. J.K., H.C., N.K. W., D.H.R., K.S., and D.B. designed mice experiments. H.C., C.J.N., and N.K.W performed mice experiments. J.K. and D.B. wrote the manuscript with input from all authors.

DECLARATION OF INTERESTS

Authors declare no competing interests.

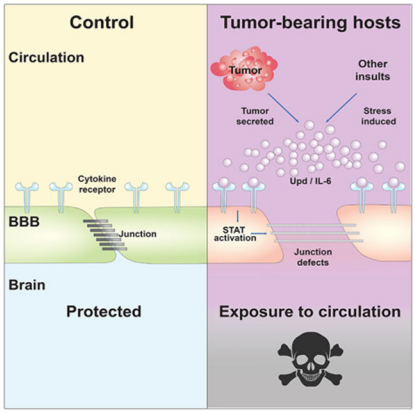

eTOC blurb

Kim et al. use a fly cancer model to uncover a systemic effect of tumors, in which inflammatory signaling permeabilizes the blood-brain barrier. Preventing barrier permeability allows flies to live longer with the same tumor burden, and key aspects of these data are recapitulated in a mouse tumor model.

INTRODUCTION

A key feature of cancer is its ability to accelerate death of the host, and this can be caused by effects at a distance from the local site of tumor growth itself (McAllister and Weinberg, 2010). Paraneoplastic syndromes such as cancer-associated cachexia and coagulopathies have enormous impacts on patient morbidity and mortality (Baracos et al., 2018, Boccaccio and Comoglio, 2009), raising the question of whether there exist additional, unrecognized mechanisms through which tumors can remotely impact host tissues with lethal consequences. Given the complexity of tumor-host interactions in native mammalian contexts, cancer models in simpler organisms such as Drosophila can contribute potential mechanisms (Figueroa-Clarevega and Bilder, 2015, Kwon et al., 2015, Song et al., 2019, Bilder et al., 2021, Newton et al., 2020, Yeom et al., 2021).

Flies have made many important contributions to understanding pathways driving oncogenesis (Bilder, 2004, Gonzalez, 2013, Chatterjee and Deng, 2019). Most of this research focused on the imaginal discs, epithelial tissues that grow in the larval stage as primordia of adult organs. Mutations in tumor suppressor genes, overexpression of oncogenes, or a combination of the two can transform disc cells into ‘neoplastic tumors’ that overproliferate, lose epithelial organization, and show defective differentiation and other tumorous characteristics. A pioneering demonstration of the malignant capabilities of Drosophila neoplasms utilized a classical allograft assay to transplant disc tissue into the abdomen of an adult host, whose open circulatory system provides a growth-permissive environment (Beadle and Ephrussi, 1935, Gateff and Schneiderman, 1969). Whereas WT discs arrest growth at their appropriate size in this assay, tumorous discs will grow uncontrollably, killing the host rapidly and robustly (Gateff and Schneiderman, 1969, Pagliarini and Xu, 2003, Rossi and Gonzalez, 2015). Allografts have been previously used to study various tumor-autonomous phenotypes (Rossi and Gonzalez, 2015), and recently

exploited to investigate tumor-host interactions (Bilder et al., 2021), but why tumors rapidly accelerate the lethality of hosts remains unknown. Here we chose to investigate these mechanisms.

RESULTS

Malignant fly tumors compromise the BBB

Allografts of malignant Drosophila epithelial tissues have long been known to induce robust and rapid lethality in hosts (Gateff and Schneiderman, 1969, Pagliarini and Xu, 2003, Rossi and Gonzalez, 2015). When transplanted into a WT adult, wing imaginal discs conditionally induced to express activated forms of the oncogenes Ras and aPKC (hereafter called 'tumors') reduce the median survival rate by >50% compared to non-oncogene-expressing control transplants (Figures 1A and B), in the absence of metastasis (Figures S1A–D). Flies dying of tumors did not show dramatic gut permeability (Figure S1E) which is associated with flies dying of old age (Clark et al., 2015), indicating a different mechanism driving mortality. We and others have shown that similar tumor models cause cachexia-like tissue wasting, due to production of an insulin antagonist with function analogous to mammalian IGFBPs (Figueroa-Clarevega and Bilder, 2015, Kwon et al., 2015). Surprisingly, depletion of this cachectogenic factor in malignant imaginal discs, which efficiently rescued wasting, did not extend lifespan of hosts bearing these tumors (Figures 1B and S1F–H). Additional unknown mechanisms must be responsible for the premature lethality induced by systemic effects of fly tumors.

We considered alternative secreted proteins that might mediate tumor-induced death. Malignant Drosophila tumors originating in several organs and driven by distinct genetic alterations show common and strong upregulation of *unpaired (upd) 1, 2*, and/or *3* (Bunker et al., 2015, Kulshammer et al., 2015, Moberg et al., 2005, Pastor-Pareja et al., 2008, Song et al., 2019, Staley and Irvine, 2010, Vaccari and Bilder, 2005, Wu et al., 2010). These three genes encode cytokines that are considered fly orthologs of IL-6, and accordingly signal through an IL-6R-like receptor called Domeless (Dome) to activate the JAK-STAT pathway in target tissues (Brown et al., 2001, Amoyel et al., 2014). Flies transplanted with tumors showed widespread activation of a STAT activity reporter throughout the abdomen, indicative of systemic inflammation (Figures 1C and D). Interestingly, this reporter was also elevated in the brain (Figures 1E–F, S1I), especially at its surface (Figure S1J). Cell type-specific markers revealed that the activated STAT signal colocalized with glial cells rather than neurons (Figure 1G). Glia also expressed high levels of Dome (Figure S1K). These data reveal that tumors activate STAT-mediated inflammatory signaling in host glial cells.

A major role of Drosophila surface glia is to serve as the blood-brain barrier (BBB), which forms a sheath around the brain and maintains homeostasis by restricting permeability from the surrounding circulatory fluid (hemolymph). Although not of endothelial origin, these cells show significant conservation both structurally and functionally with the mammalian BBB (Hindle and Bainton, 2014, O'Brown et al., 2018). As in mammals, claudin-based junctions between fly BBB cells prevent almost all paracellular diffusion into the neuropil. We tested whether tumors might alter BBB function by injecting fluorescently-labelled

10 kDa dextran into the hemolymph and measuring dye penetration into the brain 15 hours later (Pinsonneault et al., 2011). This assay is not sensitive to circadian rhythms (Figure S2A) (Zhang et al., 2018). Whereas hosts transplanted with WT imaginal discs efficiently excluded dextran from the brain, hosts carrying transplanted tumors displayed a dramatic increase in BBB permeability, with dextran signal enhanced in the brain parenchyma (Figures 2A–C). An independent malignant tumor model, driven by genetic induction of oncogenic Yorkie in adult intestinal stem cells (Kwon et al., 2015), also showed this permeable BBB phenotype (Figure S2B). Increased BBB permeability in the transplant model was first evident 12 days after tumor induction (Figure 2D). This raised the possibility that BBB defects are merely secondary consequences of animal death. However, alternative lethality-inducing conditions such as starvation or oxidative stress did not alter BBB integrity (Figures S2C and D).

The barrier function of the Drosophila BBB lies within the large, flat subperineural glia (SPG) which surround the brain (Hindle and Bainton, 2014). We examined components of the occluding intercellular junctions (septate junctions) that are formed by SPGs and limit paracellular transport. While septate junction proteins were found in narrow, dense bands between SPGs in both WT flies and hosts transplanted with control imaginal discs, septate junction proteins in tumor-transplanted hosts displayed wider and more diffuse patterns of localization (Figure 2E–F). This pattern resembles that seen in BBB-defective *moody* mutants, consistent with a disruption of BBB integrity (Bainton et al., 2005). In addition, levels of the Claudin homologs, Kune-kune and mega were decreased compared to other BBB junctional components (Figures 2E–H and S2E–H). These data suggest that transplanted tumors actively induce BBB disruption.

BBB permeability is induced by tumor-derived cytokines

To determine whether BBB permeability is caused by JAK-STAT activating ligands, we removed Upds from either host or tumor tissue. Transplants of tumors into *upd2*/*upd3* null mutant hosts, like transplants of tumors into WT hosts, caused permeation of injected dextran from the hemolymph to the brain (Figures 3A, B, D). By contrast, WT hosts transplanted with tumors depleted of *upd2* and *upd3* by RNAi maintained normal BBB function (Figure S3A). Because autocrine JAK-STAT signaling promotes tumor growth (Figure S3B) (Wu et al., 2010, Bunker et al., 2015), we also overexpressed a constitutively active form of JAK while depleting *upd2* and *upd3* in the transplanted tumor, and again found that the BBB remained intact in the presence of comparable tumor burden (Figures 3C, D, and S3C).

We further tested the necessity and sufficiency of cell-autonomous STAT activation for BBB permeabilization. Blocking STAT signaling in the BBB or SPG cells by depleting Dome or STAT with specific GAL4 drivers robustly prevented the leaky BBB phenotypes induced by tumors (Figures 3E–H). Conversely, SPG-specific overexpression of constitutively active JAK in untransplanted adults led to rapid disruption of BBB permeability (Figure 3I). Moreover, overexpression of Upd2 or Upd3 in muscle also compromised BBB permeability (Figure S3D). Taken together, the above data indicate that direct action of tumor-produced Upd cytokines on glial cells is the cause of BBB disruption.

The BBB protects fly hosts from tumor-induced death

What is the physiological consequence of tumor cytokine-induced BBB permeability? We assessed host phenotypes when STAT signaling was blocked in BBB cells and found that cachexia-like wasting was not altered (Figures S3E and F). Moreover, such manipulations had no effect on tumor size (Figure S3G). Strikingly, preventing STAT activation in BBB cells led to the extension of lifespan in tumor-bearing hosts. Median survival time was extended ~33% when Dome was depleted in all BBB cells, and by ~45% when STAT was depleted in SPG alone (Figures 3J and K). Depletion of Dome in all BBB cells or depletion of STAT in SPG cells had no positive impact on lifespan in hosts without transplants (Figures S3H and I). Consistent with this finding, WT hosts bearing *upd2/3*-depleted tumors with activated JAK, in which the BBB is intact, showed extended lifespan, whereas *upd2/3*-deficient hosts transplanted with a standard tumor still showed premature death (Figure 3L). Together, these data reveal that an intact BBB protects adult flies from lethal systemic effects of a tumor.

Is death promoted by tumors simply due to loss of core BBB functions such as ionic homeostasis? Transgenic SPG-specific STAT activation did cause premature host lethality, but death occurred long (~20 days) after the onset of BBB dysfunction (Figures 3I and M), in contrast to the synchronous kinetics seen with tumor transplants (Figure 2D). Flies depleted of the BBB junction-regulating GPCR Moody in adulthood also lived for several weeks despite brain permeability to dextran (Figures S3J and K) (Bainton et al., 2005). These results suggest that STAT-mediated BBB disruption does not alone compromise host lifespan. To verify this model, we transplanted tumors depleted of *upd2* and *upd3* into hosts whose BBB was compromised by STAT activation in SPG. *upd2/3*-depleted tumors still accelerated death of hosts in which the BBB was defective (Figure S3L). By contrast, *upd2/3*-depleted tumors transplanted into control hosts showed lifespans comparable to non-tumorous discs transplanted into control hosts (Figures 1B and S3L). Overall, our results demonstrate that JAK-STAT activation in BBB is necessary but not sufficient to cause rapid death of tumor-bearing hosts. They also hint that additional tumor-dependent factors may enter the brain to induce lethality.

A protective BBB is disrupted in other chronic inflammatory conditions

The existence of a native STAT-regulated pathway to alter BBB permeability raises the question of whether physiological stimuli other than tumors might trigger it. Endocrine upregulation of Upds has been described in two other adult contexts: microbial infection and a high-fat diet (Woodcock et al., 2015, Chakrabarti et al., 2016). We found that both infection with *E. faecalis* and lard feeding also resulted in clear permeabilization of the BBB, with STAT reporter activation and expansion of septate junction markers in SPG cells that closely resembled those seen in tumor-bearing hosts (Figures 4A–I). Moreover, when lard-fed adults were returned to a normal diet, dextran exclusion was restored (Figure 4J), revealing that this alteration in barrier permeability is reversible and not due to permanent cellular damage.

We then asked whether BBB permeability plays a functional role in protecting animals from the above insults, as it does from tumors. Lard feeding and *E. faecalis* infection are known to

reduce viability of adult flies (Woodcock et al., 2015, Chakrabarti et al., 2016). Remarkably, in both cases preventing BBB permeability through blocking STAT activation specifically in SPG cells significantly extended host lifespan (Figures 4K and L). Inflammatory opening of the BBB in these chronic conditions, as in a tumor, is therefore deleterious to the host. Together, these results demonstrate that physiological changes in BBB permeability are an important aspect of the systemic stress response, and can regulate animal survival from a variety of morbid challenges.

A mouse tumor model shows IL-6-dependent BBB permeability

To test whether tumors might systemically impact the BBB of a mammal as well, we turned to the mouse. Three weeks after implantation of B16 melanoma cells into the flank, sections through the hippocampal dentate gyrus revealed that tumor-bearing host brains showed higher levels of glial fibrillary acidic protein (GFAP) compared to controls, suggesting reactive astrocytes (Figures 5A, B, and D). Since reactive gliosis occurs in conditions including but not limited to BBB dysfunction (Yang and Wang, 2015, Liddelow and Barres, 2017), we assessed BBB function directly by tracer injection. This analysis confirmed BBB leakage: when 1 Kd NHS-Biotin was injected in the tail vein, tumor-bearing hosts showed increased extravascular levels in the brain parenchyma compared to control hosts (Figures 5E, F, and H)(O'Brown et al., 2018). Moreover, immunostaining for the junctional components Claudin-5 and Occludin revealed decreased levels in the BBB of tumor-bearing hosts (Figures 5 I, J, L and S4A, B, D).

We then explored whether this phenotype might involve IL-6-mediated inflammatory signaling, which is analogous to Upd-mediated inflammatory signaling in flies. Peripheral blood ELISAs demonstrated higher levels of circulating IL-6 in tumor-bearing hosts (Figure 6A). When these animals were subsequently injected with function-blocking antibodies against the IL-6 receptor (IL-6R), the sickness behavior and premature mortality induced by the tumor significantly improved (Figures 6C and D)(Mai et al., 2018). Comparison of hippocampal sections demonstrated that anti-IL-6R administration also caused significant decreases in both extravascular tracer intensity and reactive astrocyte induction; moreover, levels of BBB junctional components were restored (Figures 5C, D, G, H, K, L, and S4C, D). IL-6 modulates BBB permeability in other contexts (Arima et al., 2012, Rochfort and Cummins, 2015), but can also play pro-tumorigenic roles including promoting intrinsic growth and modulating the microenvironment and the anti-tumor immune response (Johnson et al., 2018, Kumari et al., 2016). Interestingly, the improved outcomes of anti-IL-6R-treated mice were not associated with a reduction of tumor burden (Figure 6B). Overall, a mammalian tumor can also compromise BBB function in an IL-6-dependent manner that promotes host morbidity.

DISCUSSION

Mechanisms of cancer lethality are multifarious and mysterious, but go well beyond the mass effect. Here we identify a paraneoplastic syndrome that in both flies and mice can promote death from cancer. In the fly, cytokines produced by distant epithelial tumors induce permeabilization of the BBB, and specifically preventing this BBB opening extends

host lifespan (Figure 6E). The systemic inflammatory environment with IL-6 family cytokine upregulation seen in tumor-bearing flies is a common phenotype induced by mammalian cancer (Johnson et al., 2018, Kumari et al., 2016, Dolan et al., 2018, Seruga et al., 2008), and our experiments demonstrate that blocking IL-6 signaling in tumor-bearing mice concomitantly rescues both BBB permeability and host morbidity without impacting tumor growth. We emphasize that we have not tested whether the beneficial effects of IL-6R antibody administration lie in its direct action on mouse BBB cells. Nevertheless, the data raise the possibility that a conserved signaling axis mediating inflammatory weakening of the BBB could contribute to mortality of certain human cancer patients. We note that a leaky BBB alone is not sufficient in flies to cause acute death; instead our results suggest that other tumor-induced factors may cross the barrier to trigger mortality.

Our data further show that additional inflammatory conditions can open the fly BBB, including a high fat diet which in mice also stimulates IL-6 upregulation and downregulation of junctional Claudins that regulate BBB permeability (Kanoski et al., 2010, Sabio et al., 2008). Since obesity is strongly associated with poor outcomes of cancer patients (Lauby-Secretan et al., 2016, Arnold et al., 2015), this raises the possibility that systemic inflammatory weakening of the BBB could be a contributing factor. Indeed, lard-fed fly hosts bearing tumors show accelerated mortality (Figure S4E). It is appealing to consider that targeting such a BBB-dependent mechanism regulating host survival could be an orthogonal clinical approach to standard tumoricidal intervention in cancer patients. Such a ‘tolerance therapy’, which addresses ultimate causes of death rather than tumor growth itself, may be less prone to selective pressures that create therapeutic resistance, and may also be agnostic to specifics of tumor tissue-of-origin or genotypes.

Limitations of the study

For technical reasons, our studies focused on female animals, but we note that effects may be less prominent in males for unknown reasons. Mouse experiments demonstrating systemic perturbation of the BBB were limited to one tumor cell line known to generate IL-6 production. Note that anti-IL6R antibody treatment of tumor-bearing mice did not target the BBB specifically; conditional knockout of STAT signaling in BBB cells of tumor-bearing mice would provide precise information on the therapeutic site of IL-6 inhibition comparable to that shown in flies.

STAR METHODS

RESOURCE AVAILABILITY

Lead contact—Further information and requests for resources and reagents should be directed to and will be fulfilled by the lead contact, David Bilder (bilder@berkeley.edu).

MATERIALS AVAILABILITY

Drosophila stains generated in this study will be available upon request from the Lead contact, David Bilder (bilder@berkeley.edu).

DATA AND CODE AVAILABILITY

This study did not generate new computational code, software, or algorithm.

EXPERIMENTAL MODEL AND SUBJECTS DETAILS

Drosophila stocks and husbandry—Gal4 drivers used included *9-137-GAL4* (‘*BBB-GAL4’,* which expresses in both SPG and PG) and *moody-GAL4* (‘*SPG-GAL4’*), along with *tubGAL80ts* to control GAL4 transactivation. Control flies were crossed to *w1118* or a *UAS-RNAi* line targeting *mCherry*. Flies were raised on cornmeal, molasses, and yeast food at room temperature unless otherwise noted. For lard feeding, 15 % lard (weight/volume) and 0.5 % agar (weight/volume) was added to food above. For oxidative stress induction, only a cotton ball soaked in 5% sucrose and 5% H_2O_2 was provided. For complete starvation, flies were placed in vials containing only a water-soaked cotton ball. For circadian rhythm synchronization, flies were kept in 25°C incubators with 12 hr light: 12 hr dark cycle for >3 generations before testing. For complete genotypes, see Table S1.

METHODS DETAILS

Drosophila tumor transplantation, gut tumor induction and infection—Before transplantation or injection, all apparatus was cleaned with 70% ethanol to minimize bacterial infection. For transplantation, wing discs from wandering 3rd instar larvae kept at room temperature were dissected into PBS. One intact disc was transplanted into the abdomen of female adult flies using a fine glass needle (Rossi and Gonzalez, 2015). Adults were then incubated at 29°C to induce transgene expression. Tumor size, ovary size, BBB permeability, and STAT-GFP were measured 15 days after transplantation and temperature shift. To genetically induce gut tumors, female *esg-Gal4, tub-Gal80^{ts}>UAS-yki^{3SA}* flies were maintained at 29°C for 15 days. Tests showed that lifespan was extended by ~ 2 days in males. For infection, newly eclosed female flies were maintained at 29°C for 5 days to allow transgene induction. *E. faecalis* was cultured in LB at 37°C overnight and 50 nl of 1:10 diluted *E. faecalis* culture, corresponding to 400–500 colony-forming units, was injected into the abdomen of CO_2-anaesthetized hosts using a Picospritzer II microinjector.

Drosophila Lifespan assays—Newly eclosed (0–24 hour) WT flies were kept at room temperature for 2 days prior to tumor transplantation, *E. faecalis* injection, or lard feeding. For lifespans involving flies with temperature-sensitive transgenes, newly eclosed adults were kept at 29°C for >4 days. Females were segregated in groups <30 individuals/vial, except for lard feeding which used only male flies to prevent larval activity from increasing food liquification. Deaths were counted daily and flies were transferred without anesthesia to new food every 2–3 days. For smurf assays, flies were raised on standard food with 2.5 % (w/v) of FD&C blue dye #1, or provided with a cotton ball soaked in 5% sucrose and 3% dextran sodium sulfate (DSS) to disrupt the gut (Rera et al., 2012).

Measurement of BBB permeability and brain imaging in Drosophila—Using a fine glass needle, ~100 nl of 25 mg/ml 10,000 MW TR-dextran was injected in the abdomen of adult females. If tumor-bearing hosts were bloated, excess hemolymph was removed using a glass needle. 15 hours after dextran injection, flies were fixed in 4% paraformaldehyde for 80 minutes and washed in 0.1% PBST before brain dissection. Brains

were imaged using a Zeiss LSM 700 confocal microscope on the same day of fixation to minimize diffusion of dextran. Average intensity was measured in a confocal section from the central plane of the brain at two regions using ImageJ. STAT-GFP intensity was quantitated in the optic lobes via a maximum intensity projection taken at 2 um intervals. Immunohistochemistry followed standard protocols. To quantify anti-Kune and anti-Mega stainings and NrxIV-GFP, and Nrg-GFP, the intensity plot profile of lines (10 um) across each bicellular segment of the septate junctions was measured and the area below the profile was calculated using ImageJ.

Preparation and handling of tumor-bearing mice—C57BL/6J mice were purchased from the Jackson Laboratory. All mice used were aged 10 to 15 weeks. B16-F10 cells were cultured under standard conditions (Marcus et al., 2018). Cells were washed and resuspended in PBS, and 100 ul containing 1×10^6 cells was injected subcutaneously. Mice used as controls received only PBS subcutaneously. For anti-IL-6R antibody treatment, mice received either PBS or anti-IL-6R (200 ug, Intraperitoneal injection) starting on day 9 and repeated every three days until mice were sacrificed. Sickness behavior was assayed according to (Mai et al., 2018). Tests suggested that female mice showed greater sickness behavior than male mice, so females were subsequently analyzed. Tumor growth was measured using calipers, and tumor volume was estimated using the ellipsoid formula: $V=(\pi/6)ABC$. All experiments were approved by the University of California Berkeley Animal Care and Use Committee.

Mouse brain imaging and measurement of IL-6 levels—Mice were sacrificed at 21 days or earlier when required by IACUC guidelines. For immunohistochemistry alone, mice were anesthetized and transcardially perfused with 10 ml of PBS and 20 ml of 4% paraformaldehyde (PFA) at a rate of 2 ml/min. The brains were dissected and postfixed with 4% PFA at 4°C overnight. For tracers, mice were injected intravenously with 0.2 mg/g body weight Sulfo-NHS-Biotin dissolved in 0.9% sterile saline in the lateral tail vein. Fifteen minutes after injection, brains were dissected and drop-fixed in 4% paraformaldehyde (PFA) overnight at 4 °C. All brains were cryoprotected in 30% sucrose in PBS for 48 hr, embedded in tissue freezing medium, and then stored at −80 °C. Frozen brains were cryostat sectioned at the thickness of 30 um, mounted on slides and stored at −20°C until processed. Immunohistochemistry, Biotin detection and mounting followed standard protocols and samples were imaged on a Zeiss 700 confocal microscope. For each mouse, >5 sections of the dentate gyrus of the hippocampus were analyzed; values shown are intensity averages of sections analyzed in the hilar region. Leakage of Sulfo-NHS-Biotin into brain parenchyma was quantified using FIJI ImageJ software to determine the integrated fluorescence intensity outside of CD31-labelled vasculature. A staining failure in CD31/Biotin staining on sections from one tumor-bearing mouse led to this sample being discarded. Claudin and Occludin levels were quantified as mean intensity of hilar region signal following subtraction of background measured in non-vascular neuropil. For IL-6 level measurements, blood was collected by cardiac puncture from control and tumor-bearing mice. IL-6 was quantified from harvested serum using an ELISA kit following the manufacturer’s instructions.

QUANTIFICATION AND STATISTICAL ANALYSIS

Quantification—Quantification is described in the Methods section.

Statistical analysis—The Prism (Graphpad) program was used to run statistical tests. Lifespan curves were analyzed using Log-rank test, and scatter plots were analyzed using Student's t-test (comparing 2 groups) or one-way ANOVA with Tukey post-test (comparing more than 3 groups). Kruskal-Wallis test was used to analyze nonparametric clincal score. *P<0.05, **P<0.01, ***P<0.001. Error bar represents mean ± s.d. of normalized values to control.

Supplementary Material

Refer to Web version on PubMed Central for supplementary material.

ACKNOWLEDGMENTS

We thank Roland Bainton, Chenghua Gu, Iswar Hariharan, Daniela Kaufer, Brittany Flowers, Laura Attardi and Kristin Scott for advice and discussion. We acknowledge generous gifts of reagents from Matthias Behr, Greg Beitel, Christian Klambt, Frederic Geissmann, Terry Orr-Weaver, Amita Sehgal, Laurent Seugnet, Mark Van Doren, Frederick Wolf, Tian Xu and Naoki Yamanaka and the community resources provided by TRiP at Harvard Medical School (NIH/NIGMS R01-GM084947), the Bloomington Drosophila Stock Center (NIH P40OD018537) and the Vienna Drosophila Resource Center. This work was supported by NIH grants GM090150 and GM130388 to D.B, AI113041 to D.H.R, and HD092093 to K.S., as well as an NSF Graduate Research Fellowship 1752814 to N.K.W, NIH fellowship F31CA228381 to C.J.N and a Pew Scholarship to K.S.

REFERENCES

AMOYEL M, ANDERSON AM & BACH EA 2014. JAK/STAT pathway dysregulation in tumors: a Drosophila perspective. Semin Cell Dev Biol, 28, 96–103. [PubMed: 24685611]

ARIMA Y, HARADA M, KAMIMURA D, PARK JH, KAWANO F, YULL FE, KAWAMOTO T, IWAKURA Y, BETZ UA, MARQUEZ G, BLACKWELL TS, OHIRA Y, HIRANO T & MURAKAMI M 2012. Regional neural activation defines a gateway for autoreactive T cells to cross the blood-brain barrier. Cell, 148, 447–57. [PubMed: 22304915]

ARNOLD M, PANDEYA N, BYRNES G, RENEHAN PAG, STEVENS GA, EZZATI PM, FERLAY J, MIRANDA JJ, ROMIEU I, DIKSHIT R, FORMAN D & SOERJOMATARAM I 2015. Global burden of cancer attributable to high body-mass index in 2012: a population-based study. Lancet Oncol, 16, 36–46. [PubMed: 25467404]

BAINTON RJ, TSAI LT, SCHWABE T, DESALVO M, GAUL U & HEBERLEIN U 2005. moody encodes two GPCRs that regulate cocaine behaviors and blood-brain barrier permeability in Drosophila. Cell, 123, 145–56. [PubMed: 16213219]

BARACOS VE, MARTIN L, KORC M, GUTTRIDGE DC & FEARON KCH 2018. Cancer-associated cachexia. Nat Rev Dis Primers, 4, 17105. [PubMed: 29345251]

BEADLE GW & EPHRUSSI B 1935. Transplantation in Drosophila. Proc Natl Acad Sci U S A, 21, 642–6. [PubMed: 16588024]

BILDER D 2004. Epithelial polarity and proliferation control: links from the Drosophila neoplastic tumor suppressors. Genes Dev, 18, 1909–25. [PubMed: 15314019]

BILDER D, ONG K, HSI TC, ADIGA K & KIM J 2021. Tumor-host interactions through the lens of Drosophila. Nature Reviews Cancer, 10.1038/s41568-021-00387-5.

BOCCACCIO C & COMOGLIO PM 2009. Genetic link between cancer and thrombosis. J Clin Oncol, 27, 4827–33. [PubMed: 19738115]

BROWN S, HU N & HOMBRIA JC 2001. Identification of the first invertebrate interleukin JAK/STAT receptor, the Drosophila gene domeless. Curr Biol, 11, 1700–5. [PubMed: 11696329]

BUNKER BD, NELLIMOOTTIL TT, BOILEAU RM, CLASSEN AK & BILDER D 2015. The transcriptional response to tumorigenic polarity loss in Drosophila. Elife, 4.

CHAKRABARTI S, DUDZIC JP, LI X, COLLAS EJ, BOQUETE JP & LEMAITRE B 2016. Remote Control of Intestinal Stem Cell Activity by Haemocytes in Drosophila. PLoS Genet, 12, e1006089. [PubMed: 27231872]

CHATTERJEE D & DENG WM 2019. Drosophila Model in Cancer: An Introduction. Adv Exp Med Biol, 1167, 1–14. [PubMed: 31520346]

CLARK RI, SALAZAR A, YAMADA R, FITZ-GIBBON S, MORSELLI M, ALCARAZ J, RANA A, RERA M, PELLEGRINI M, JA WW & WALKER DW 2015. Distinct Shifts in Microbiota Composition during Drosophila Aging Impair Intestinal Function and Drive Mortality. Cell Rep, 12, 1656–67. [PubMed: 26321641]

DOLAN RD, LAIRD BJA, HORGAN PG & MCMILLAN DC 2018. The prognostic value of the systemic inflammatory response in randomised clinical trials in cancer: A systematic review. Crit Rev Oncol Hematol, 132, 130–137. [PubMed: 30447918]

FIGUEROA-CLAREVEGA A & BILDER D 2015. Malignant Drosophila tumors interrupt insulin signaling to induce cachexia-like wasting. Dev Cell, 33, 47–55. [PubMed: 25850672]

GATEFF E & SCHNEIDERMAN HA 1969. Neoplasms in mutant and cultured wild-tupe tissues of Drosophila. Natl Cancer Inst Monogr, 31, 365–97. [PubMed: 5374686]

GONZALEZ C 2013. Drosophila melanogaster: a model and a tool to investigate malignancy and identify new therapeutics. Nat Rev Cancer, 13, 172–83. [PubMed: 23388617]

HINDLE SJ & BAINTON RJ 2014. Barrier mechanisms in the Drosophila blood-brain barrier. Front Neurosci, 8, 414. [PubMed: 25565944]

JOHNSON DE, O'KEEFE RA & GRANDIS JR 2018. Targeting the IL-6/JAK/STAT3 signalling axis in cancer. Nat Rev Clin Oncol, 15, 234–248. [PubMed: 29405201]

KANOSKI SE, ZHANG Y, ZHENG W & DAVIDSON TL 2010. The effects of a high-energy diet on hippocampal function and blood-brain barrier integrity in the rat. J Alzheimers Dis, 21, 207–19. [PubMed: 20413889]

KULSHAMMER E, MUNDORF J, KILINC M, FROMMOLT P, WAGLE P & UHLIROVA M 2015. Interplay among Drosophila transcription factors Ets21c, Fos and Ftz-F1 drives JNK-mediated tumor malignancy. Dis Model Mech, 8, 1279–93. [PubMed: 26398940]

KUMARI N, DWARAKANATH BS, DAS A & BHATT AN 2016. Role of interleukin-6 in cancer progression and therapeutic resistance. Tumour Biol, 37, 11553–11572. [PubMed: 27260630]

KWON Y, SONG W, DROUJININE IA, HU Y, ASARA JM & PERRIMON N 2015. Systemic organ wasting induced by localized expression of the secreted insulin/IGF antagonist ImpL2. Dev Cell, 33, 36–46. [PubMed: 25850671]

LAUBY-SECRETAN B, SCOCCIANTI C, LOOMIS D, GROSSE Y, BIANCHINI F, STRAIF K & INTERNATIONAL AGENCY FOR RESEARCH ON CANCER HANDBOOK WORKING, G. 2016. Body Fatness and Cancer--Viewpoint of the IARC Working Group. N Engl J Med, 375, 794–8. [PubMed: 27557308]

LIDDELOW SA & BARRES BA 2017. Reactive Astrocytes: Production, Function, and Therapeutic Potential. Immunity, 46, 957–967. [PubMed: 28636962]

MAI SHC, SHARMA N, KWONG AC, DWIVEDI DJ, KHAN M, GRIN PM, FOX-ROBICHAUD AE & LIAW PC 2018. Body temperature and mouse scoring systems as surrogate markers of death in cecal ligation and puncture sepsis. Intensive Care Med Exp, 6, 20. [PubMed: 30054760]

MARCUS A, MAO AJ, LENSINK-VASAN M, WANG L, VANCE RE & RAULET DH 2018. Tumor-Derived cGAMP Triggers a STING-Mediated Interferon Response in Non-tumor Cells to Activate the NK Cell Response. Immunity, 49, 754–763 e4. [PubMed: 30332631]

MCALLISTER SS & WEINBERG RA 2010. Tumor-host interactions: a far-reaching relationship. J Clin Oncol, 28, 4022–8. [PubMed: 20644094]

MOBERG KH, SCHELBLE S, BURDICK SK & HARIHARAN IK 2005. Mutations in erupted, the Drosophila ortholog of mammalian tumor susceptibility gene 101, elicit non-cell-autonomous overgrowth. Dev Cell, 9, 699–710. [PubMed: 16256744]

NEWTON H, WANG YF, CAMPLESE L, MOKOCHINSKI JB, KRAMER HB, BROWN AEX, FETS L & HIRABAYASHI S 2020. Systemic muscle wasting and coordinated tumour response drive tumourigenesis. Nat Commun, 11, 4653. [PubMed: 32938923]

O'BROWN NM, PFAU SJ & GU C 2018. Bridging barriers: a comparative look at the blood-brain barrier across organisms. Genes Dev, 32, 466–478. [PubMed: 29692355]

PAGLIARINI RA & XU T 2003. A genetic screen in Drosophila for metastatic behavior. Science, 302, 1227–31. [PubMed: 14551319]

PASTOR-PAREJA JC, WU M & XU T 2008. An innate immune response of blood cells to tumors and tissue damage in Drosophila. Dis Model Mech, 1, 144–54; discussion 153. [PubMed: 19048077]

PINSONNEAULT RL, MAYER N, MAYER F, TEGEGN N & BAINTON RJ 2011. Novel models for studying the blood-brain and blood-eye barriers in Drosophila. Methods Mol Biol, 686, 357–69. [PubMed: 21082381]

RERA M, CLARK RI & WALKER DW 2012. Intestinal barrier dysfunction links metabolic and inflammatory markers of aging to death in Drosophila. Proc Natl Acad Sci U S A, 109, 21528–33. [PubMed: 23236133]

ROCHFORT KD & CUMMINS PM 2015. The blood-brain barrier endothelium: a target for pro-inflammatory cytokines. Biochem Soc Trans, 43, 702–6. [PubMed: 26551716]

ROSSI F & GONZALEZ C 2015. Studying tumor growth in Drosophila using the tissue allograft method. Nat Protoc, 10, 1525–34. [PubMed: 26357008]

SABIO G, DAS M, MORA A, ZHANG Z, JUN JY, KO HJ, BARRETT T, KIM JK & DAVIS RJ 2008. A stress signaling pathway in adipose tissue regulates hepatic insulin resistance. Science, 322, 1539–43. [PubMed: 19056984]

SERUGA B, ZHANG H, BERNSTEIN LJ & TANNOCK IF 2008. Cytokines and their relationship to the symptoms and outcome of cancer. Nat Rev Cancer, 8, 887–99. [PubMed: 18846100]

SONG W, KIR S, HONG S, HU Y, WANG X, BINARI R, TANG HW, CHUNG V, BANKS AS, SPIEGELMAN B & PERRIMON N 2019. Tumor-Derived Ligands Trigger Tumor Growth and Host Wasting via Differential MEK Activation. Dev Cell, 48, 277–286 e6. [PubMed: 30639055]

STALEY BK & IRVINE KD 2010. Warts and Yorkie mediate intestinal regeneration by influencing stem cell proliferation. Curr Biol, 20, 1580–7. [PubMed: 20727758]

VACCARI T & BILDER D 2005. The Drosophila tumor suppressor vps25 prevents nonautonomous overproliferation by regulating notch trafficking. Dev Cell, 9, 687–98. [PubMed: 16256743]

WOODCOCK KJ, KIERDORF K, POUCHELON CA, VIVANCOS V, DIONNE MS & GEISSMANN F 2015. Macrophage-derived upd3 cytokine causes impaired glucose homeostasis and reduced lifespan in Drosophila fed a lipid-rich diet. Immunity, 42, 133–44. [PubMed: 25601202]

WU M, PASTOR-PAREJA JC & XU T 2010. Interaction between Ras(V12) and scribbled clones induces tumour growth and invasion. Nature, 463, 545–8. [PubMed: 20072127]

YANG Z & WANG KK 2015. Glial fibrillary acidic protein: from intermediate filament assembly and gliosis to neurobiomarker. Trends Neurosci, 38, 364–74. [PubMed: 25975510]

YEOM E, SHIN H, YOO W, JUN E, KIM S, HONG SH, KWON DW, RYU TH, SUH JM, KIM SC, LEE KS & YU K 2021. Tumour-derived Dilp8/INSL3 induces cancer anorexia by regulating feeding neuropeptides via Lgr3/8 in the brain. Nat Cell Biol, 23, 172–183. [PubMed: 33558728]

ZHANG SL, YUE Z, ARNOLD DM, ARTIUSHIN G & SEHGAL A 2018. A Circadian Clock in the Blood-Brain Barrier Regulates Xenobiotic Efflux. Cell, 173, 130–139. [PubMed: 29526461]

Highlights

- Fly tumors induce paraneoplastic opening of the blood-brain barrier (BBB)
- BBB permeabilization by tumor-induced Jak/STAT activation accelerates host death
- BBB also protects flies from high-fat diet and non-pathogenic infections
- A mouse tumor model disrupts the protective BBB in an IL-6-dependent manner

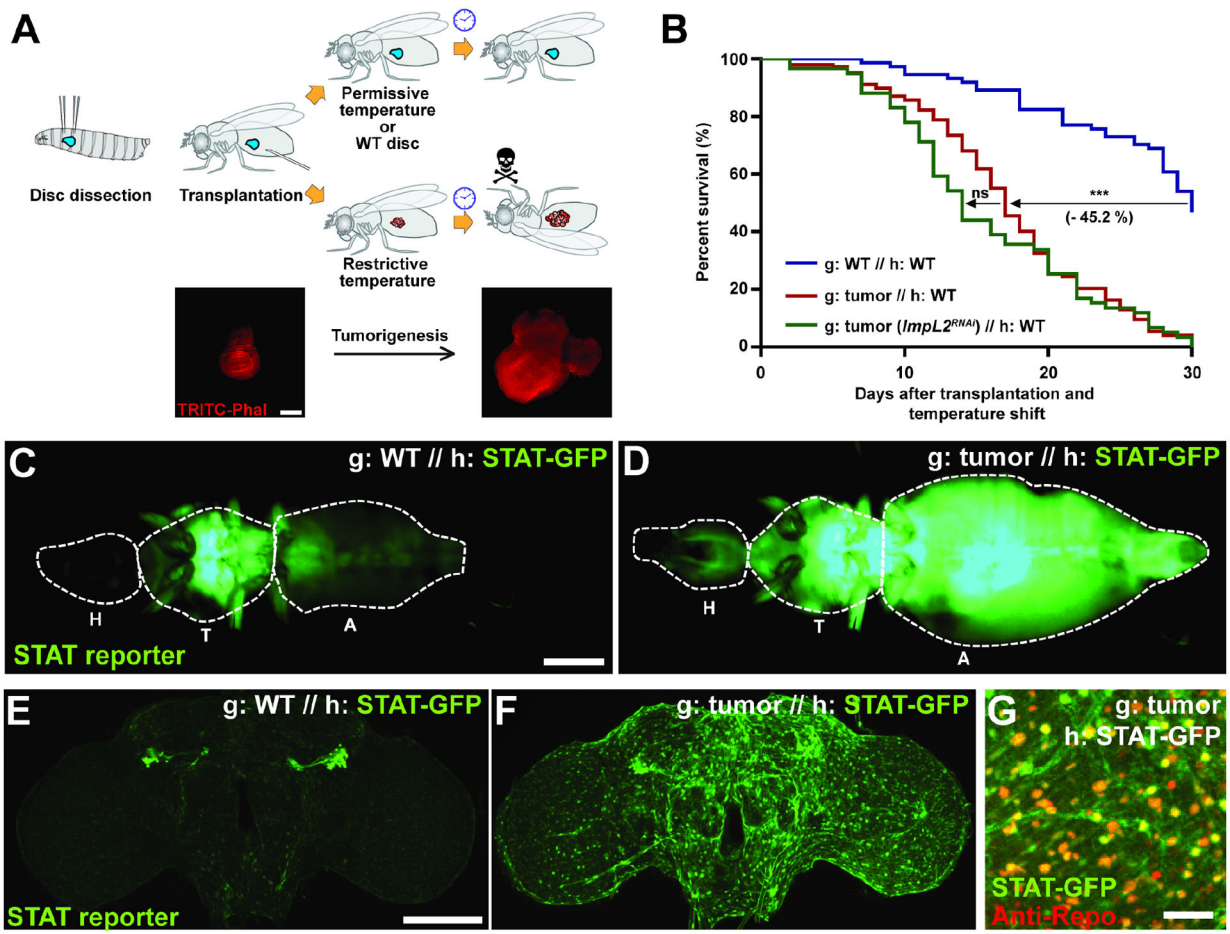

Figure 1. Tumor-bearing fly hosts show glial Jak/STAT activation and premature death.

(A) Procedure to allograft tissue conditionally expressing oncogenes, with images of wing discs prior to shift to restrictive temperature and after 15 days in host following shift. Scale bar, 150 um. **(B)** Lifespans of hosts (h) with various graft (g) transplants. Tumor-bearing host (red, n=147) lifespan is reduced compared to hosts with control grafts (blue, n=74). Depletion of the wasting factor *ImpL2* from tumor does not rescue host lifespan (green, n=59). **(C, D)** Tumor causes systemic activation of Jak/STAT signaling in hosts, especially in the head. H: head; T: thorax; A: abdomen. Scale bar, 500 um. **(E, F)** Elevated STAT activity in the brain of tumor hosts, shown by maximum intensity projection. Scale bar, 100 um. **(G)** STAT reporter colocalizes with Repo staining, which labels glial cells. Scale bar, 20 um.

Lifespan curves; *P<0.05, **P<0.01, ***P<0.001, not significant (ns)P>0.05; Log-rank test.

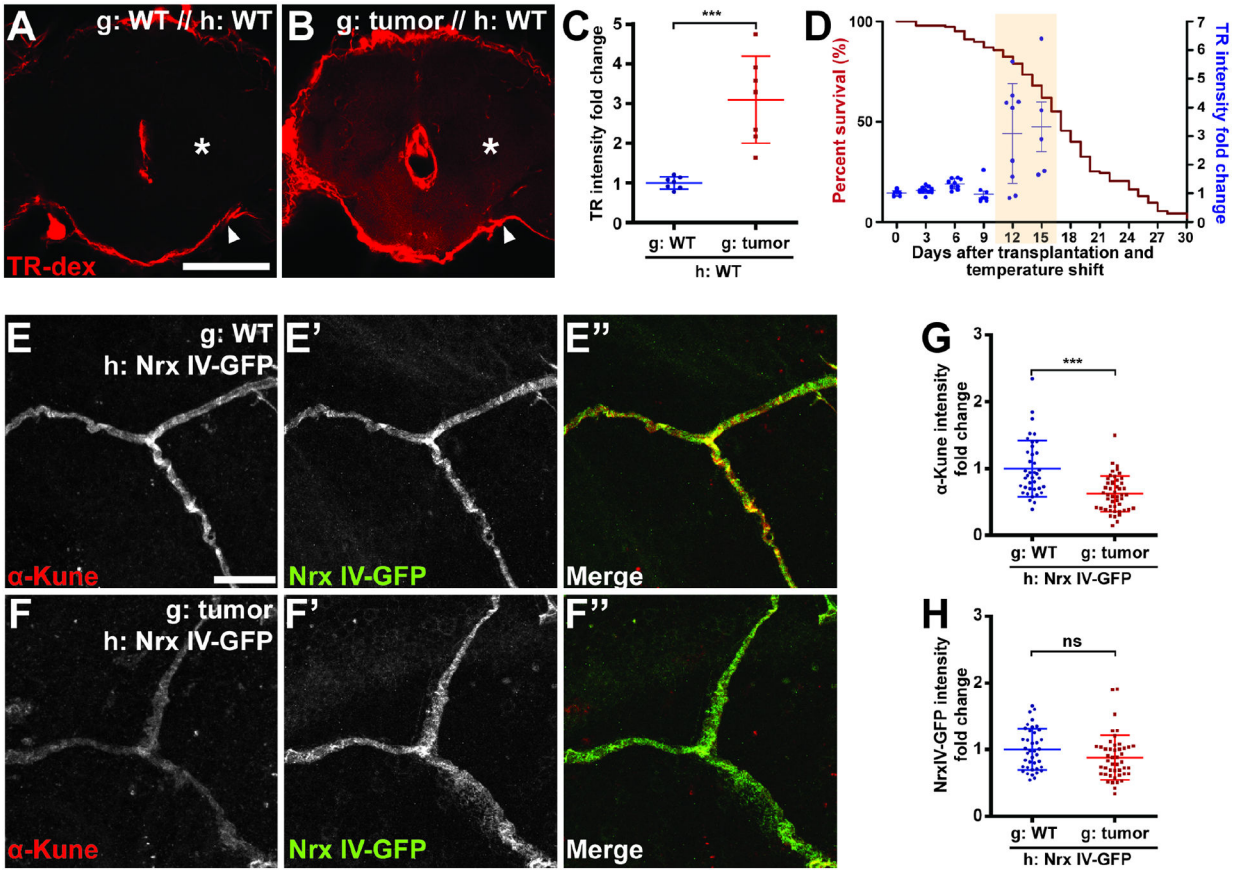

Figure 2. Fly tumors induce BBB disruption.

(A, B) BBB protects the brain from TR-dextran (TR-dex) penetration in control hosts, but TR-dex passes through the BBB of tumor-bearing hosts. Asterisks indicate parenchyma of brain, which is covered by BBB indicated by arrowheads. Scale bar, 100 um. **(C)** Quantification of TR-dex intensity in the brain (n=7 each). **(D)** Correlation between kinetics of BBB permeability (blue dots) and lifespan curve (red line) of tumor-bearing hosts (n≥5 each). Shaded region shows days when BBB permeability is detected. **(E, F)** Diffuse septate junctions of BBB cells in brains of tumor hosts compared to control. Scale bar, 10 um. **(G, H)** Intensity of the junctional claudin Kune but not the junctional protein NrxIV is decreased in the brain of tumor vs control hosts (n=81, 79).

Scattered plots; *P<0.05, **P<0.01, ***P<0.001, not significant (ns)P>0.05; Student's t-test. Error bar represents mean±s.d. of normalized values to control.

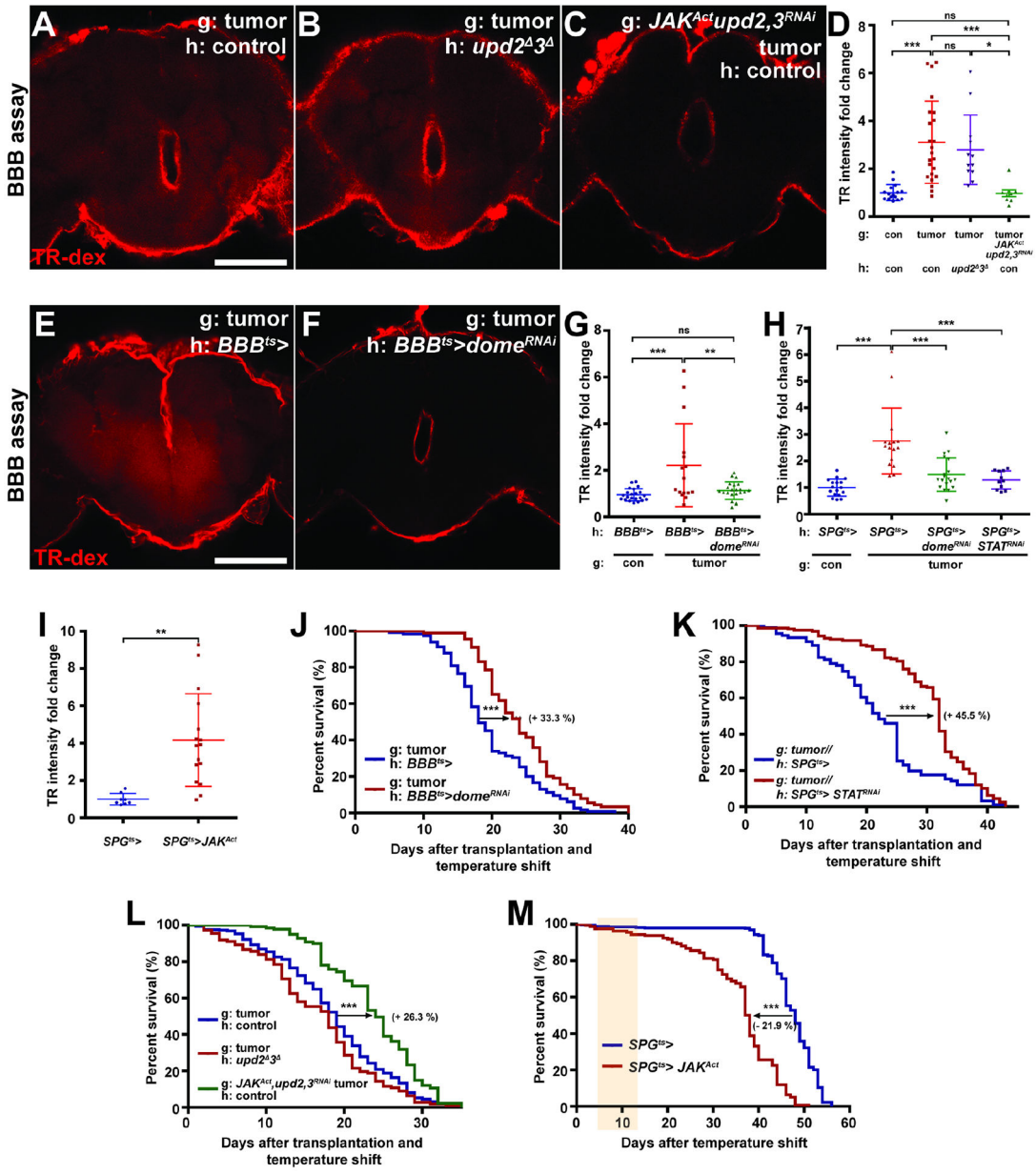

Figure 3. Jak/STAT inhibition rescues tumor-induced BBB permeability and extends host lifespan.

(A–D) Tumor-bearing hosts of control genotype (A) or tumor-bearing hosts that lack *upd2* and *upd3* (B) show permeable BBB, but depletion of *upd2* and *upd3* in transplanted tumors rescues the permeable BBB phenotype (C, activated JAK is coexpressed to restore autocrine growth). Scale bar, 100 um. (D) Quantification of TR-dex intensity in the brain of genotypes shown in (A) (red, n=23), (B) (purple, n=12), (C) (green, n=5), and non-tumor control (blue, n=16). **(E, F)** Inhibition of Jak/STAT pathway in BBB cells (via *dome-RNAi)* rescues permeability of BBB in tumor hosts. **(G)** Quantification of TR-dex intensity in the brain of genotypes shown in (E) (red, n=16), (F) (green, n=22), and non-tumor control (blue, n=22). Scale bar, 100 um. **(H)** Depleting Dome (green, n=19) or STAT (purple, n=11) in the SPG cells rescues permeable BBB in tumor-bearing hosts compared to tumor-bearing

hosts expressing GAL4 only (red, n=16). Values are normalized to non-tumor control (blue, n=17). **(I)** Ectopic activation of Jak/STAT in SPG (red, n=16) is sufficient to open BBB compared to control (blue, n=8) at day 5 after temperature shift. **(J)** Inhibition of Jak/STAT pathway in BBB (red, n=89) extends lifespan of tumor-bearing hosts compared to control (blue, n=115). **(K)** Lifespan extension of tumor-bearing hosts with STAT depletion in SPG (red, n=158) compared to control (blue, n=91). **(L)** Control hosts bearing tumors lacking *upd2* and *upd3* (green, n=102) show extended lifespan compared to *upd2/upd3* null hosts bearing control tumor (red, n=112) or control hosts bearing control tumor (blue, n=265). **(M)** Tissue-specific ectopic activation of Jak/STAT pathway in SPG (red, n=160) reduces lifespan compared to control (blue, n=358). Shaded region shows days after BBB permeability is detected (cf **3I**).

Scattered plots represent mean±s.d of normalized values to control. *P<0.05, **P<0.01, ***P<0.001, not significant (ns)P>0.05; One-way anova (Tukey post test) for (D), (G) and (H), Student's t-test for (I). Lifespan curves; *P<0.05, **P<0.01, ***P<0.001, not significant (ns)P>0.05; Log-rank test. Error bar represents mean±s.d of normalized values to control.

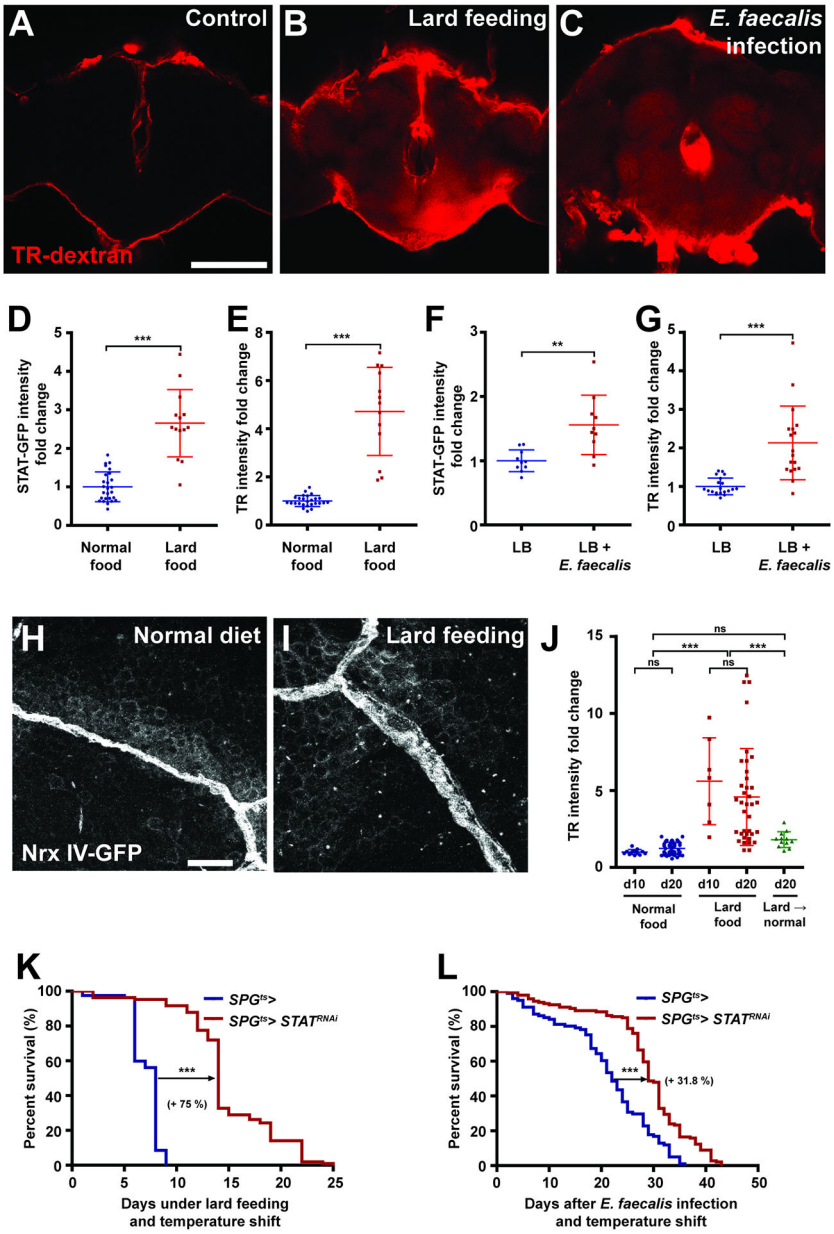

Figure 4. BBB permeability regulates survival to chronic physiological insults.

(A–C) Representative brain images of control (A), lard-fed (B), or *E. faecalis* infected (C) with TR-dex injection. Scale bar, 100 um. **(D, E)** High fat diet (red, n=14) increases brain STAT reporter intensity and TR-dex penetration compared to control (blue, n=26 each). **(F, G)** Injection of *E. faecalis* (red, n=10) increases brain STAT reporter intensity and TR-dex permeability compared to control (blue, n=10). **(H, I)** Septate junctions visualized by Nrx-IV-GFP shows diffuse organization under high fat diet compared to control. Scale bar, 10 um. **(J)** Permeable BBB under high fat diet is rescued by subsequent normal food feeding. (n>7 each). **(K, L)** Depleting STAT in SPG extends lifespan of flies fed high fat diet (red, n=107) (K) or infected with *E. faecalis* (red, n=146) (L) compared to control (blue, n=82 and n=101, respectively).

Scattered plots; *P<0.05, **P<0.01, ***P<0.001, not significant (ns)P>0.05; Student's t-test for (D–G), one-way anova (Tukey post test) for (J). Lifespan curves; *P<0.05, **P<0.01, ***P<0.001, not significant (ns)P>0.05; Log-rank test. Error bar represents mean±s.d of normalized values to control.

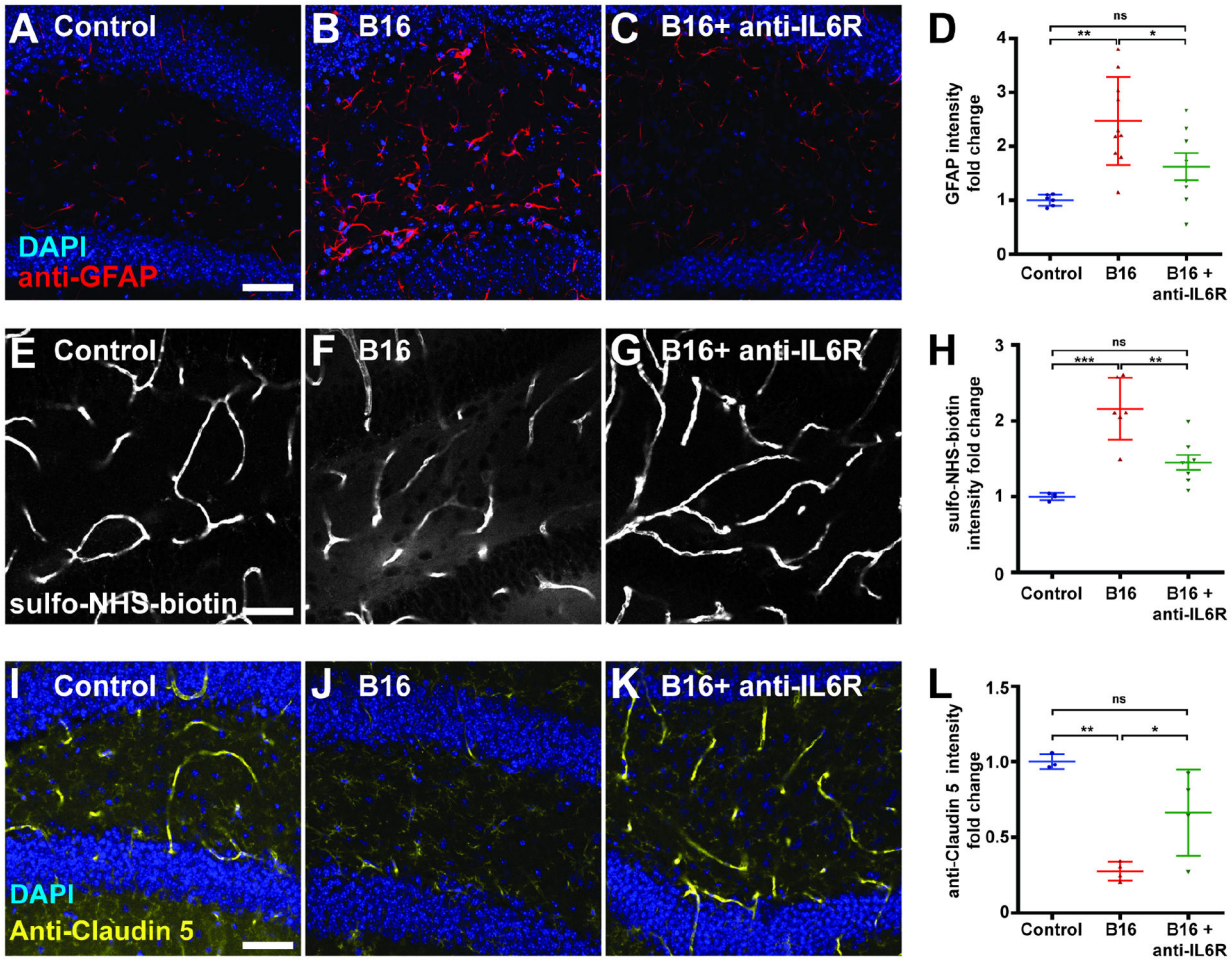

Figure 5. Paraneoplastic BBB breakdown in an IL-6-inducing mouse tumor model.

(A–D) Compared to control (A, n=6), brains of mice bearing transplanted B16-F10 melanoma cells (B, n=10) show reactive astrocytes with GFAP upregulation (red, DAPI in blue). This phenotype is reversed when tumor-bearing mice are treated with anti-IL-6R antibody (C, n=7). Scale bar, 50 um. (D) shows quantitation.

(E–H) Compared to control (E, n=4), brains of tumor-bearing mice (F, n=6) show increased BBB permeability demonstrated by extravascular presence of intravenously injected sulpho-NHS-biotin. This phenotype is reversed when tumor-bearing mice are treated with anti-IL-6R antibody (G, n=7). (H) shows quantitation.

(I–L) Compared to control (I, n=3), brains of tumor-bearing mice (J, n=4) show decreased staining of the endothelial tight junction component Claudin-5. This phenotype is reversed when tumor-bearing mice are treated with anti-IL-6R antibody (K, n=4). (L) shows quantitation.

Scattered plots; *P<0.05, **P<0.01, ***P<0.001, not significant (ns)P>0.05; one-way anova (Tukey post test). Error bar represents mean±s.d of normalized values to control.

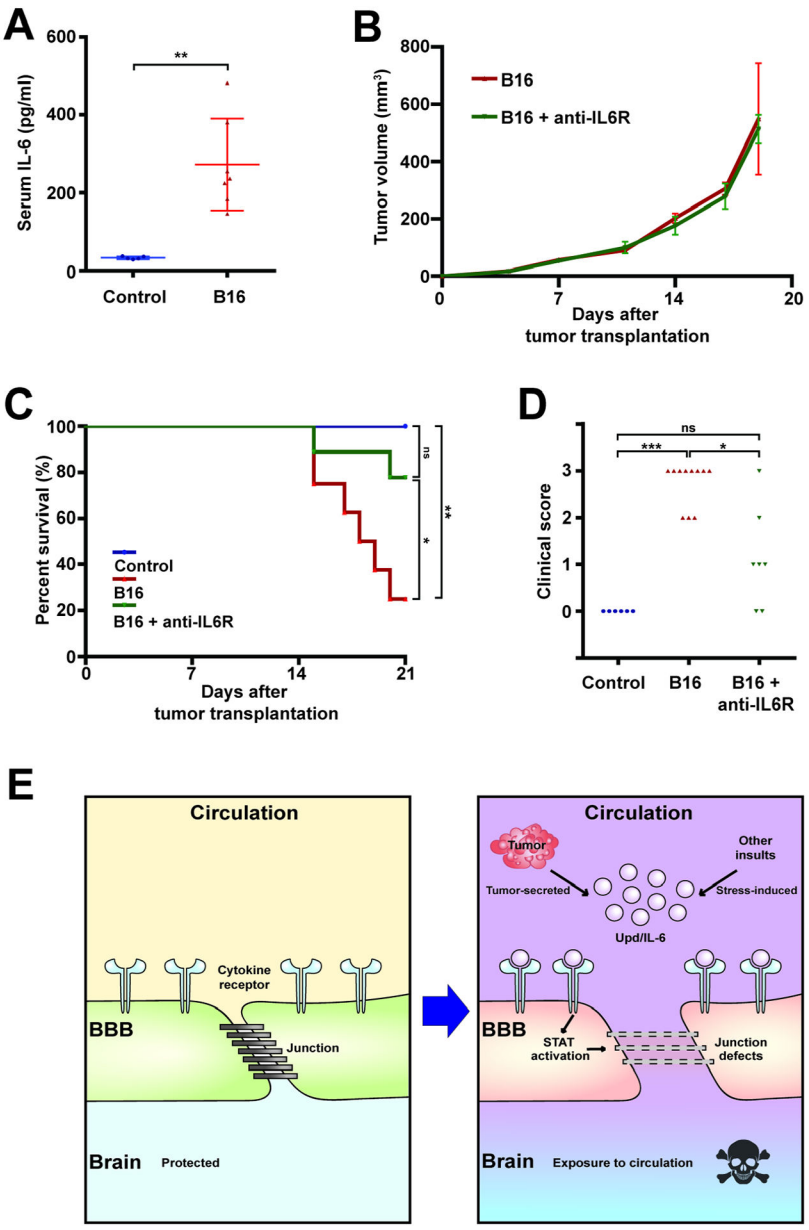

Figure 6. IL-6 inhibition ameliorates mouse tumor morbidity associated with BBB dysfunction.

(A) Elevated levels of serum IL-6 in tumor-transplanted (red, n=7) vs control (blue, n=5) mice after 3 weeks.

(B) Tumor volume is unchanged by anti-IL-6R antibody administration (green, n=8) compared to control (red, n=8).

(C, D) Anti-IL-6R antibody administration significantly rescues both survival (C) and sickness behavior (D, clinical score of 0 indicates healthy animal) of tumor-bearing mice. Control; blue, n=6, B16; red, n=10, B16+anti-IL6R; green, n=7.

(E) Model of death elicited by inflammation-mediated BBB breakdown induced by tumors, infection, or high-fat diet.

Scattered plots; *P<0.05, **P<0.01, ***P<0.001, not significant (ns)P>0.05; Student's t-test for (A, B), Kruskal-Wallis test for (D). Lifespan curves; *P<0.05, **P<0.01, ***P<0.001, not significant (ns)P>0.05; Log-rank test. Error bar represents mean±s.d of normalized values to control.

KEY RESOURCE TABLE

REAGENT or RESOURCE	SOURCE	IDENTIFIER
Antibodies		
Mouse anti-Repo (1:250)	DSHB	8D12 Anti-Repo
Rabbit anti-GFP (1:30,000)	Molecular Probes	A6455
Rabbit anti-Kune (1:250)	Gift from Dr. Beitel Northwestern University	Nelson et al. 2010
Mouse anti-Mega (1:250)	Gift from Dr. Behr Leipzig University	Behr et al. 2003
Rabbit anti-CD31 (1:50)	Abcam	Ab28364
Goat anti-GFAP (1:1,000)	Abcam	Ab53554
Mouse IL-6 ELISA MAX Standard Set	BioLegend	431301
Rat anti-IL-6R (200 ug/injection)	BioXCell	BE0047
Mouse anti-Claudin-5 (10 ug/mL)	ThermoFisher Scientific	35-2500
Mouse anti-Occludin (3 ug/mL)	ThermoFisher Scientific	33-1500
Bacterial and virus strains		
E. faecalis	Lazzaro lab Cornell University	N/A
C57BL/6J mice	Jackson Laboratory	#000664
B16-F10 melanoma cell line	UC Berkeley Cell Culture Facility	B16-F10
Chemicals, peptides, and recombinant proteins		
TRITC-Phalloidin (1:250)	Sigma-Aldrich	P1951; RRID: AB_2315148
DAPI (1:10,000)	ThermoFisher Scientific	D1306, RRID: AB_2629482
10 kDa Texas red-Dextran (25 mg/ml)	ThermoFisher Scientific	D1863
FD&C Blue #1	Spectrum Chemical MFG. Corp.	FD110
Hydrogen peroxide	Fisher Chemical	H325-100
Dextran sulfate sodium	MP Biomedicals	9011-18-1
Dulbecco's modified Eagle's medium	ThermoFisher Scientific	11995-065
Fetal bovine serum (FBS)	Omega Scientific	FB-01
Glutamine	Sigma-Aldrich	G8540
Penicillin-Streptomycin	ThermoFisher Scientific	15140-122
Gentamycin sulfate	Lonza	MT30-005-cR
β-mercaptoethanol	EMD Biosciences	21985-023
Hepes	ThermoFisher Scientific	BP310-100
PBS	ThermoFisher Scientific	14190-250
Tissue freezing medium	General data healthcare	TFM-C
Normal donkey serum	Jackson ImmunoResearch Laboratories	017-000-001
ProLong Gold Antifade mountant	ThermoFisher Scientific	P36930
EZ-Link™ Sulfo-NHS-LC-Biotin	ThermoFisher Scientific	21335
Experimental models: Organisms/strains		
Nub-Gal4	Bloomington Drosophila Stock Center	Flybase ID: FBst0086108
tubGAL80ts	Bloomington Drosophila Stock Center	Flybase ID: FBst0007018

REAGENT or RESOURCE	SOURCE	IDENTIFIER
UAS-Ras ^{v12}	Bloomington Drosophila Stock Center	Flybase ID: FBst0004847
UAS-aPKC $^{\Delta N}$	Bloomington Drosophila Stock Center	Flybase ID: FBst0051673
w ^{1118}	Bloomington Drosophila Stock Center	Flybase ID: FBst0005905
UAS-impL2^{RNAi} (validated in PMID:27633989)	Vienna Drosophila Resource Center	Flybase ID: FBst0458731
10XStat92E-GFP	Perrimon lab Harvard University	Flybase ID: FBst0026197
NrxIV-GFP	Bloomington Drosophila Stock Center	Flybase ID: FBst0050798
Nrg-GFP	Bloomington Drosophila Stock Center	Flybase ID: FBst0006844
upd2 $^{\Delta}$, *upd3* $^{\Delta}$	Bloomington Drosophila Stock Center	Flybase ID: FBst0055729
UAS-upd2^{RNAi} (validated in PMID:23021220)	Bloomington Drosophila Stock Center	Flybase ID: FBst0033949
UAS-upd3^{RNAi} (validated in PMID:25601202)	Vienna Drosophila Resource Center	Flybase ID: FBst0478692
9-137-Gal4 (BBB-Gal4)	Bainton lab University of California-San Franscisco	Flybase ID: FBti0202073
UAS-dome^{RNAi} (validated in PMID:28045022)	Vienna Drosophila Resource Center	Flybase ID: FBti0118756
Moody-Gal4 (SPG-Gal4)	Bainton lab University of California-San Franscisco	Flybase ID: FBtp0022847
UAS-Hop ^{Tum}	Perrimon lab	Flybase ID: FBal0043128
UAS-STAT^{RNAi} *(X)* (validated in PMID:17803358)	Bloomington Drosophila Stock Center	Flybase ID: FBst0026899
UAS-STAT^{RNAi} *(II)* (validated in PMID:26690827)	Vienna Drosophila Resource Center	Flybase ID: FBst0478803
10X UAS-mCD8-GFP	Bloomington Drosophila Stock Center	Flybase ID: FBst0032184
UAS-nls-GFP	Bloomington Drosophila Stock Center	Flybase ID: FBst0004775
Dome-Gal4	Bloomington Drosophila Stock Center	Flybase ID: FBst0081010
Esg-Gal4	Perrimon lab Harvard University	Flybase ID: FBti0013268
UAS-yki $^{3SA\ (S111A.S168A.S250A)}$	Bloomington Drosophila Stock Center	Flybase ID: FBst0028817
UAS-nls-GFP	Bloomington Drosophila Stock Center	Flybase ID: FBst0004776
Mef2-Gal4	Bloomington Drosophila Stock Center	Flybase ID: FBst0027390
UAS-upd2	Harrison lab University of Kentucky	Flybase ID: FBtp0110532
UAS-upd3	Harrison lab University of Kentucky	Flybase ID: FBtp0110533
UAS-mCh ^{RNAi}	Bloomington Drosophila Stock Center	Flybase ID: FBst0035787
UAS-moody^{RNAi} (validated in PMID:33307547)	Vienna Drosophila Resource Center	Flybase ID: FBst0481265
Software and algorithms		
Fiji	ImageJ	http://fiji.sc/
Illustrator	Adobe	www.adobe.com/products/illustrator.html
Photoshop	Adobe	www.adobe.com/products/photoshopfamily.html
Acrobet DC	Adobe	acrobat.adobe.com/us/en/acrobat.html
Excel	Microsoft	https://products.office.com/enus/excel
Prism	Graphpad	www.graphpad.com/scientificsoftware/prism/
Zen	Zeiss	www.zeiss.com/microscopy/us/products/microscopesoftware/zen.html